Benchmark Solutions for Three-Dimensional Transient Heat Transfer in Two-Dimensional Environments Via the Time Fourier Transform

Julieta António[1,2], António Tadeu[2], Luís Godinho[2], Nuno Simões[2]

Abstract: The evaluation of heat propagation in the time domain generated by transient heat sources placed in the presence of three-dimensional media requires the use of computationally demanding numerical schemes. The implementation of numerical 3D solutions may benefit from the existence of benchmark solutions to test the accuracy of approximate schemes.

With this purpose in mind, this article presents analytical-numerical solutions to evaluate the heat-field elicited by monopole heat sources in the presence of three different inclusions, namely, a cylindrical circular solid inclusion, a cylindrical circular cavity with null fluxes and a cavity with null temperatures prescribed along its boundary, buried in an unbounded medium. The problem is first subjected to a time and space Fourier Transform, which allows the solution to be obtained in the frequency domain as summation of 2D solutions for different spatial wavenumbers. Then, using the inverse Fourier transforms in the wavenumber and frequency domains, the 3D time responses are synthesized. Complex frequencies are used to avoid the aliasing phenomena.

This methodology is first validated calculating the fundamental time solutions for one, two and three dimensions in an unbounded medium. Simulation analyses of these idealized models are then used to study the patterns of heat propagation in the vicinity of the inclusions.

1 Introduction

The propagation of heat through inclusions and irregular boundaries is a fundamental problem in many fields, including the thermal engineering, building physics, and non-destructive testing. In some of these areas, interest is usually focused on the inverse problem: as heat travels through a medium with spatially varying thermal prop-

erties, its propagation varies giving rise to reflected heat fields. These variations are recorded by appropriately located receptors and the problem is how to use features of the records to infer the structure and properties of the medium.

For inclusions with simple geometry, for example spheres, the solution of the heat diffusion equation can be obtained by separation of variables. The same technique does not work for anisotropic and inhomogeneous media, for which the solution to the heat equation is also much more difficult to obtain computationally. The Finite Differences and Finite Element Methods require full discretization of the space under consideration and are computationally demanding. Approaches using Boundary Elements reduce the computational effort, since they require discretization only of the surfaces along material discontinuities. However, the solution of three-dimensional transient heat problems is still hard to implement and remains computationally demanding.

The solution becomes much simpler if the medium is two-dimensional (2D), even if the heat source remains three-dimensional (3D), for example a point. The solution can be obtained by means of a temporal and spatial Fourier transform in the direction in which the geometry does not vary. This involves solving a sequence of 2D problems with different spatial wavenumbers, k_z, and frequencies. Then, using the inverse Fourier transforms, in the frequency and k_z wavenumber domain, the 3D field in the time domain can be synthesized.

This method is practical for inclusions whose geometry is simple, such as circular cylinder, for which the equation is separable. The solution at each frequency is expressed in terms of heat terms with varying wavenumber k_z, (with z being the cylindrical axis), which is subsequently Fourier-transformed into the spatial domain. The wavenumber transform in discrete form is obtained by considering an infinite number of virtual point sources equally spaced along the z axis, at a sufficient distance

---

[1] Corresponding author. Tel.: +351 239 797 196; fax: +351 239 797 190. E-mail adress: julieta@dec.uc.pt

[2] Department of Civil Engineering, University of Coimbra, Polo II, 3030-290 Coimbra, Portugal

from each other to avoid spatial contamination (e.g. Bouchon and Aki (1977), Tadeu, Antonio and Simoes(2004). The analysis uses complex frequencies to avoid the aliasing phenomenon and to minimize the influence of the neighboring fictitious sources (e.g. Phinney (1965)).

In this work the exact solution is used to obtain the heat generated by monopole heat sources as they illuminate cylindrical inclusions buried in an unbounded medium. Three different inclusions are used, namely a cylindrical inclusion, a cavity with null fluxes and a cavity for which null temperatures are prescribed along its boundary.

A short presentation of the three-dimensional problem formulation is given in the next section of this article. First, the analytical solutions used to compute the frequency domain responses are described, followed by the details of the procedure used to obtain time domain results. The present expressions are validated by comparing the results obtained for one, two and three dimensional heat sources in an unbounded medium with those given by analytical fundamental solutions in the time domain. To conclude, a selection of numerical examples is presented, to show the main aspects of the heat propagation.

2   3D problem formulation

The transient heat conduction in solids can be described by the diffusion equation

$$\nabla^2 T = \frac{1}{K}\frac{\partial T}{\partial t} \tag{1}$$

where $\nabla^2 = \left(\frac{\partial^2}{\partial r^2} + \frac{1}{r}\frac{\partial}{\partial r} + \frac{1}{r^2}\frac{\partial^2}{\partial \theta^2} + \frac{\partial^2}{\partial z^2}\right)$, $r = \sqrt{x^2 + y^2}$, θ is the azimuth, t is time, $T(t, r, \theta, z)$ is temperature, $K = \frac{k}{\rho c}$ is the thermal diffusivity, k is the thermal conductivity, ρ is the density and c is the specific heat. Fourier transforming the time domain expression gives the Helmholtz equation in the frequency domain

$$\left(\nabla^2 + \left(\sqrt{\frac{-i\omega}{K}}\right)^2\right)\hat{T}(\omega, r, \theta, z) = 0 \tag{2}$$

where $i = \sqrt{-1}$ and ω is the frequency. Eq. (2) is analogous to the one used to solve acoustic problems where $\omega/(velocity\ of\ pressure\ waves)$ corresponds to $\sqrt{\frac{-i\omega}{K}}$ in the diffusion equation. In this way, the transient heat

propagation solution can be understood as a propagation of heat waves.

Eq. (2) can be solved for a heat point source ($p(x, y, z, t) = \delta(x)\delta(y)\delta(z)e^{i(\omega t)}$ where $\delta(x)$, $\delta(y)$ and $\delta(z)$ are Dirac-delta functions) in an unbounded medium, located at the origin of the coordinate system, to give the fundamental solution

$$\hat{T}_f(\omega, r, \theta, z) = \frac{1}{2k\sqrt{r^2 + z^2}}e^{-\sqrt{\frac{i\omega}{K}}\sqrt{r^2 + z^2}} \tag{3}$$

The computation of 3D problems is, in many cases, very costly in terms of computer effort. If the geometry of the problem remains constant along one direction (z) the solution becomes simpler, expressing the full 3D problem as a summation of 2D solutions with different spatial k_z wavenumbers (e.g. Tadeu and Kausel (2000)). This is implemented applying a Fourier transformation along the z direction. Applying this procedure to equation (2) leads to the following equation

$$\left(\tilde{\nabla}^2 + \left(\sqrt{\frac{-i\omega}{K} - (k_z)^2}\right)^2\right)\tilde{T}(\omega, r, \theta, k_z) = 0 \tag{4}$$

with $\tilde{\nabla}^2 = \left(\frac{\partial^2}{\partial r^2} + \frac{1}{r}\frac{\partial}{\partial r} + \frac{1}{r^2}\frac{\partial^2}{\partial \theta^2}\right)$.

The fundamental solution of this equation is in turn obtained by applying a spatial Fourier transform in the z direction to the fundamental solution equation for a heat point source (Eq.(3)),

$$\tilde{T}_f(\omega, r, \theta, k_z) = \frac{-i}{4k}H_0\left(\sqrt{\frac{-i\omega}{K} - (k_z)^2}\ r\right) \tag{5}$$

where $H_n()$ are Hankel functions of the second kind and order n. This equation can be interpreted as the response to a spatially varying heat line source of the form $p(x, y, z, t) = \delta(x)\delta(y)e^{i(\omega t - k_z z)}$ (see Fig. 1).

The full three-dimensional solution is synthesized applying an inverse Fourier transform along the k_z direction. The inverse Fourier transformation can be written as a discrete summation, if one assumes the existence of virtual sources equally spaced, L, along z. The solution can thus be obtained by solving a limited number of two-dimensional problems.

$$\hat{T}(\omega, r, \theta, z) = \frac{2\pi}{L}\sum_{m=-M}^{M}\tilde{T}(\omega, r, \theta, k_{zm})e^{-ik_{zm}z} \tag{6}$$
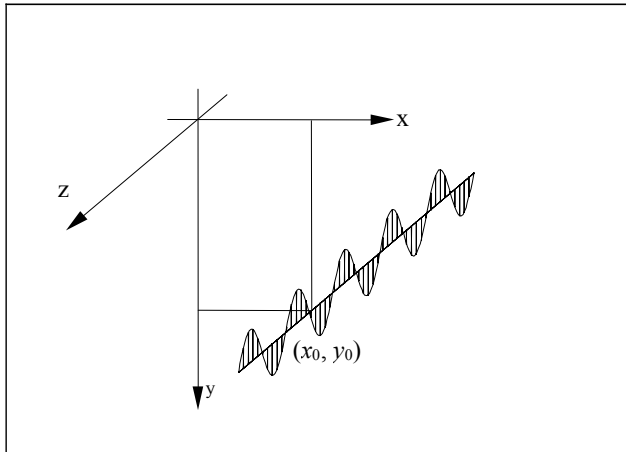
Figure 1 : Spatially harmonic varying line load.

with k_{zm} being the axial wavenumber given by $k_{zm} = \frac{2\pi}{L}m$. The distance L must be large enough to avoid spatial contamination from the virtual sources [Bouchon and Aki (1977)]. An analogous technique has been used by the authors to study wave propagation inside seismic prospecting boreholes [Tadeu, Godinho, and Santos (2002)] and the outdoor propagation of sound waves in the presence of obstacles [Godinho, António, and Tadeu (2001)].

These equations can be written as a continuous superposition of heat plane sources. Eq. (5) is then rendered by the expression,

$$\tilde{T}_f(\omega, x, y, k_z) = \frac{-i}{4\pi\,k} \int\limits_{-\infty}^{+\infty} \left(\frac{e^{-iv|y-y_0|}}{v}\right) e^{-ik_x(x-x_0)}dk_x \quad (7)$$

where $v = \sqrt{\frac{-i\omega}{K} - k_z^2 - k_x^2}$ with $(Im(v) \leq 0)$, and the integration is performed with respect to the horizontal wavenumber (k_x) along the x direction.

This integral is transformed into a summation by using an infinite number of sources distributed along the x direction, at equal intervals L_x. The above equation can then be written as

$$\tilde{T}_f(\omega, x, y, k_z) = E_0 \sum_{n=-\infty}^{n=+\infty} \left(\frac{E}{v_n}\right) E_d \quad (8)$$

where $E_0 = \frac{-i}{2kL_x}$, $E = e^{-iv_n|y-y_0|}$, $E_d = e^{-ik_{xn}(x-x_0)}$, $v_n = \sqrt{\frac{-i\omega}{K} - k_z^2 - k_{xn}^2}$ with $(Im(v_n) \leq 0)$, $k_{xn} = \frac{2\pi}{L_x}n$,

which can in turn be approximated by a finite sum of equations (N).

Notice that $k_z = 0$ corresponds to the two-dimensional case.

3 Validation of the spatial and time Fourier transformation

The procedure described in the previous section was implemented and validated by applying it to the calculation of the one, two and three-dimensional fundamental solutions for a unit heat source placed in an unbounded medium in the time domain. The exact solution of Eq. (1) in an unbounded medium in the time domain, when a unit heat source is applied at point (x_0, y_0, z_0) at time $t = t_0$, is

$$T(t, x, y, z) = \frac{1}{\rho c\,(4\pi K\tau)^{d/2}} e^{\left(-\frac{r_{00}^2}{4K\tau}\right)} \text{ if } t > t_0 \quad (9)$$

where $\tau = t - t_0$, r_{00} is the distance between the source point and the field point (x, y, z), and $d = 3$, $d = 2$ and $d = 1$ when in the presence of a three, two and one-dimensional problem, respectively [Carslaw and Jaeger (1959)].

The results obtained with Eq. (9) for a unit heat source, are compared with those given above: for a plane source $(d = 1)$, ascribing $k_z = 0$ and $k_{xn} = 0$ to Eq. (8); for a cylindrical source $(d = 2)$, using Eq. (5), ascribing $k_z = 0$ multiplied by L_x, and spherical $(d = 3)$ calculated using Eq. (3), divided by 2π. The thermal material properties ascribed to the homogeneous unbounded solid medium used in this validation are $k = 63.9\,\text{W.m}^{-1}.^{o}\text{C}^{-1}$, $c = 434.0\,\text{J.Kg}^{-1}.^{o}\text{C}^{-1}$ and $\rho = 7832.0\,\text{Kg.m}^{-3}$. At time $t = 2.78\,\text{h}$, a unit heat source is excited at $(x = 0.0\,\text{m}, y = 0.0\,\text{m}, z = 0.0\,\text{m})$. Fig. 3 displays the temperature computed along a line of 40 receivers placed from $y = -1.5\,\text{m}$ to $y = 1.5\,\text{m}$, (see Fig. 2) for a plane, cylindrical and spherical unit heat source, at different times.

Computations are performed in the frequency range $[0,1024\text{x}10^{-5}\,\text{Hz}]$ with a frequency increment of $\Delta\omega = 10^{-5}\,\text{Hz}$, which defines a time window of $T = 27.78\,\text{h}$. Complex frequencies of the form $\omega_c = \omega - 0.7i\Delta\omega$ have been used to avoid the aliasing phenomenon. In Fig. 3 the marks represent the response computed using the proposed Green's functions, and the solid line displays the solution given by Eq. (9). The agreement between these two solutions is excellent.
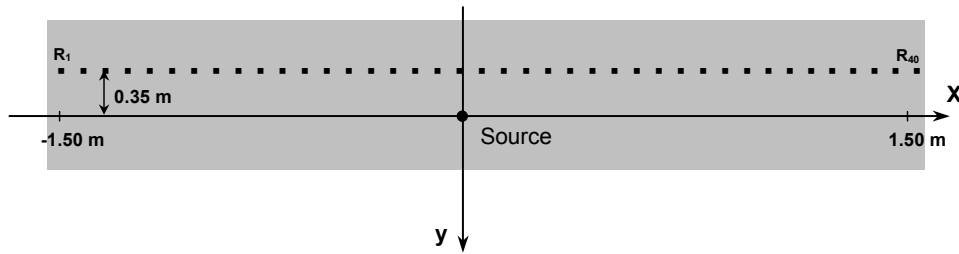
Figure 2 : Geometry of the problem.

4   Analytical solution

4.1   Solid inclusion

Consider first a spatially uniform solid medium (1) of infinite extent (with a thermal conductivity k_1, a density ρ_1 and a specific heat c_1), having buried within it a cylindrical inclusion (2) (with a thermal conductivity k_2, a density ρ_2 and a specific heat c_2), with radius a. This is subjected to a harmonic monopole heat source at an off-center position $(x_0, 0, 0)$, placed in the exterior medium, oscillating with a frequency ω as illustrated in Fig. 1. The heat diffusion generated by this source propagates and hits the surface of the buried inclusion. After reaching the outer surface of the inclusion, part of the incident heat energy is reflected back to the exterior solid medium, and the remaining energy is transmitted into the solid material inclusion.

Incident heat field (or free-field)

The three dimensional incident field generated by a monopole heat source, placed at $(x_0,0,0)$, outside the inclusion, satisfies Eq. (2), and can be expressed as

$$\hat{T}_{inc}(\omega,r') = \frac{A}{2k_1\,r'}e^{-\sqrt{\frac{i\omega}{K_1}}r'} \text{ with}$$

$$r' = \sqrt{(x-x_0)^2 + y^2 + z^2} \tag{10}$$

where the subscript *inc* denotes the incident field, A is the heat amplitude, $K_1 = \frac{k_1}{\rho_1\,c_1}$ and r' defines the distance between the source and the receiver. When a Fourier transformation is applied along the z direction, the incident field can be expressed as a summation of 2D sources, with different spatial wavenumbers,

$$\hat{T}_{inc}(\omega,r') = \frac{2\pi}{L}\sum_{m=-M}^{M}\tilde{T}_{inc}(\omega,r,k_{zm})\,e^{-ik_{zm}z} \tag{11}$$

with $\tilde{T}_{inc}(\omega,r,k_{zm}) = \frac{-iA}{4k_1}H_0\left(k_{\alpha_1}\,r''\right),$ $r'' = \sqrt{(x-x_0)^2 + y^2}$ and $k_{\alpha_1} = \sqrt{\frac{-i\omega}{K_1} - (k_{zm})^2}$.

Eq. (11) poses a difficulty, however, because it expresses the incident field in terms of heat terms centered at the source point $(x_0, 0, 0)$, and not at the axis of the cylindrical inclusion. This problem can be overcome by expressing the incident heat field in terms of heat terms centered at the origin, which can be achieved by using Graf's addition theorem [Watson (1980)], to give the expressions (in cylindrical coordinates):

$$\tilde{T}_{inc}(\omega,r,\theta,k_{zm})$$
$$= -\frac{iA}{4k_1}\sum_{n=0}^{\infty}(-1)^n\varepsilon_n H_n(k_{\alpha_1}r_0)J_n(k_{\alpha_1}r)\cos(n\theta)$$
when $r < r_0$ \hfill (12)

$$\tilde{T}_{inc}(\omega,r,\theta,k_{zm})$$
$$= -\frac{iA}{4k_1}\sum_{n=0}^{\infty}(-1)^n\varepsilon_n J_n(k_{\alpha_1}r_0)H_n(k_{\alpha_1}r)\cos(n\theta)$$
when $r > r_0$ \hfill (13)

in which r_0 is the distance from the source to the axis of the inclusion, $J_n(\dots)$ are Bessel functions of order n and

$$\varepsilon_n = \left\{ \begin{array}{lll} 1 & if & n=0 \\ 2 & if & n\neq 0 \end{array} \right. .$$

Reflected heat field in the exterior region

In the frequency-axial-wavenumber domain, the reflected heat field in the exterior region can be expressed in a form similar to that of the incident field, namely

$$\tilde{T}_{ref}(\omega,r,\theta,k_{zm}) = \sum_{n=0}^{\infty}A_n H_n(k_{\alpha_1}r)\cos(n\theta) \tag{14}$$

in which the subscript *ref* denotes the reflected heat field, and A_n is an as yet unknown coefficient to be determined

a)

b)

c)
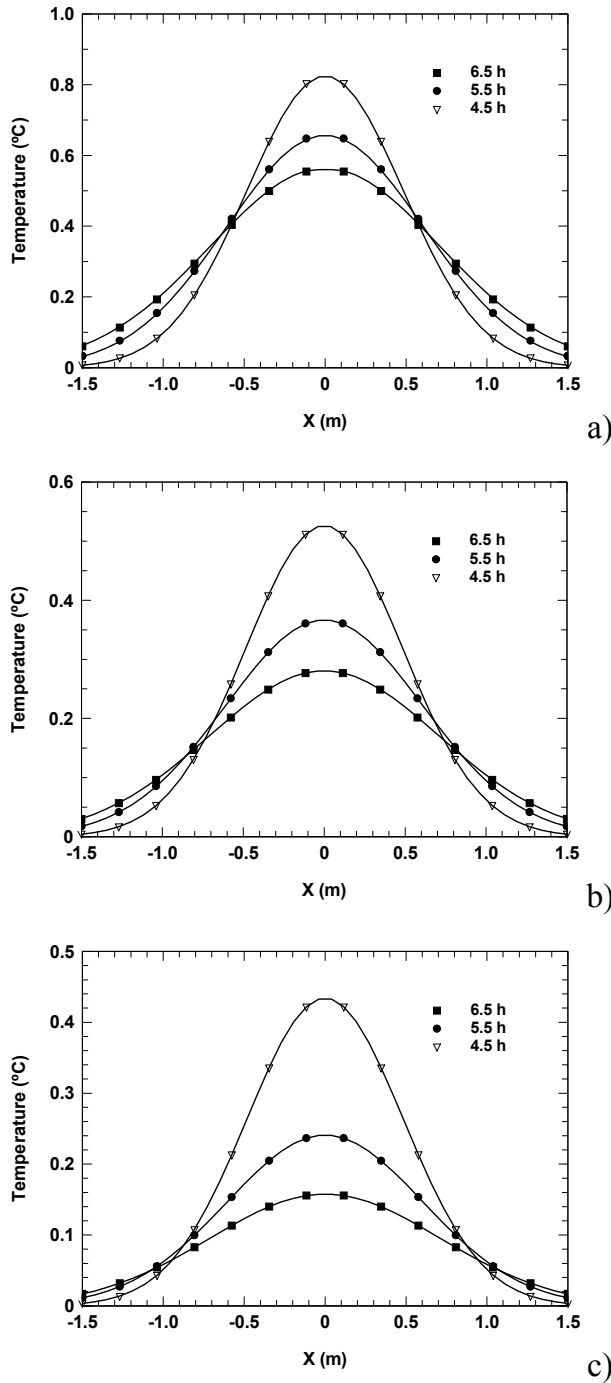
Figure 3 : Temperature along a line of 40 receivers, at different times (4.5 h, 5.5 h and 6.5 h): a) for a plane ($d = 1$) unit heat source; b) for a cylindrical ($d = 2$) unit heat source; c) for a spherical ($d = 3$) unit heat source.

from appropriate boundary conditions. Together with an implicit factor $e^{i(\omega t - k_z z)}$, the Hankel functions in Eq. (14) represent diverging or outgoing cylindrical heat field.

Transmitted heat field in the interior region

The transmitted heat field in the inclusion can be expressed as:

$$\tilde{T}_{trans}(\omega, r, \theta, k_{zm}) = \sum_{n=0}^{\infty} B_n J_n(k_{\alpha_2} r) \cos(n\theta) \quad (15)$$

in which the subscript *trans* denotes the transmitted heat field, $k_{\alpha_2} = \sqrt{\frac{-i\omega}{K_2} - (k_{zm})^2}$, $K_2 = \frac{k_2}{\rho_2 c_2}$, B_n is again an unknown coefficient to be determined by imposing the appropriate boundary conditions

Definition of A_n and B_n

Next, appropriate boundary conditions are established to obtain the reflected and transmitted heat fields within the solid inclusion; that is, the continuity of temperatures and normal heat fluxes at the solid-solid interface,

$$\tilde{T}_{inc}(\omega, a, \theta, k_{zm}) + \tilde{T}_{ref}(\omega, a, \theta, k_{zm}) = \tilde{T}_{trans}(\omega, a, \theta, k_{zm})$$

$$k_1 \frac{\partial \left[\tilde{T}_{inc}(\omega, a, \theta, k_{zm}) \right]}{\partial r} + k_1 \frac{\partial \left[\tilde{T}_{ref}(\omega, a, \theta, k_{zm}) \right]}{\partial r}$$

$$= k_2 \frac{\partial \left[\tilde{T}_{trans}(\omega, a, \theta, k_{zm}) \right]}{\partial r} \quad (16)$$

Combining Eqs. (12), (13), (14) and (15) one obtains a system of equations which is then used to find the coefficients A_n and B_n,

$$\begin{bmatrix} a_{11} & a_{12} \\ a_{21} & a_{22} \end{bmatrix} \begin{bmatrix} A_n \\ B_n \end{bmatrix} = \frac{iA}{4k_1} (-1)^n \varepsilon_n H_n(k_{\alpha_1} r_0) \begin{bmatrix} b_1 \\ b_2 \end{bmatrix} \quad (17)$$

with

$$a_{11} = H_n(k_{\alpha_1} a)$$

$$a_{21} = n H_n(k_{\alpha_1} a) - (k_{\alpha_1} a) H_{n+1}(k_{\alpha_1} a)$$

$$a_{12} = -J_n(k_{\alpha_2} a)$$

$$a_{22} = \frac{k_2}{k_1} \left[-n J_n(k_{\alpha_2} a) + (k_{\alpha_2} a) J_{n+1}(k_{\alpha_2} a) \right]$$

$$b_1 = J_n(k_{\alpha_1} a)$$

$$b_2 = n J_n(k_{\alpha_1} a) - (k_{\alpha_1} a) J_{n+1}(k_{\alpha_1} a)$$
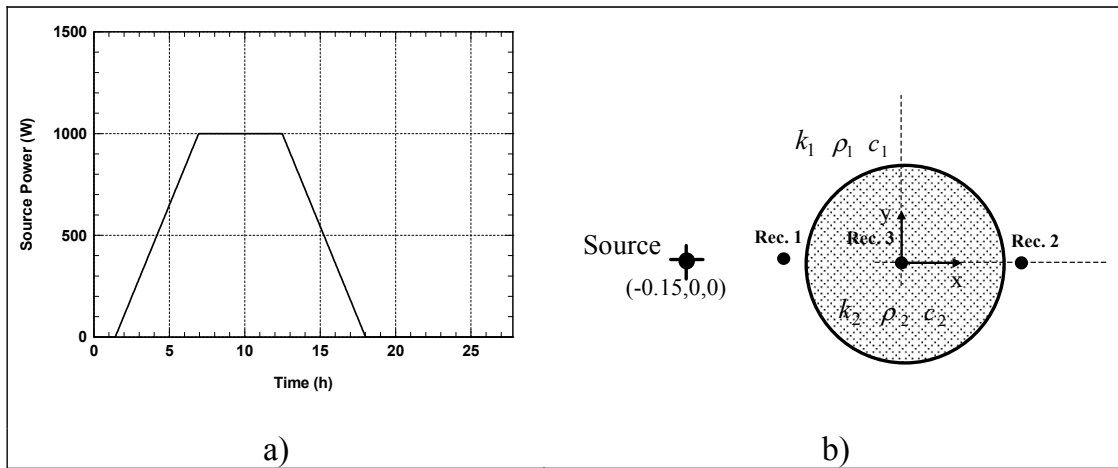
Figure 4 : a) Temporal evolution of the heat source; b) Geometry of the problem.

The coefficients A_n and B_n with the series solutions (Eqs. (14) and (15)) can now be used to determine the reflected and the transmitted heat of the system.

The solution for heat source excited in the interior can be obtained in a similar way by changing the incident field and again ascribing the continuity of temperatures and normal heat fluxes at the solid-solid interface.

4.2 Cavity with null fluxes along its boundary

The incident heat field is all reflected back into the unbounded medium, verifying the condition at $r = a$,

$$k_1 \frac{\partial \left[\tilde{T}_{inc}(\omega, a, \theta, k_{zm}) \right]}{\partial r} + k_1 \frac{\partial \left[\tilde{T}_{ref}(\omega, a, \theta, k_{zm}) \right]}{\partial r} = 0 \quad (18)$$

Under this condition the transmitted heat field is null. Therefore the solution is found combining Eqs. (12) and (14), so as to satisfy Eq. (18). When this is done, one obtains,

$$A_n =$$
$$\frac{\frac{-i}{4k_1} (-1)^n \varepsilon_n H_n(k_{\alpha_1} r_0) \left[-n J_n(k_{\alpha_1} a) + (k_{\alpha_1} a) J_{n+1}(k_{\alpha_1} a) \right]}{n H_n(k_{\alpha_1} a) - (k_{\alpha_1} a) H_{n+1}(k_{\alpha_1} a)}$$

$$(19)$$

4.3 Cavity with null temperatures along its boundary

At the surface of the cavity $(r = a)$ the boundary condition is given by,

$$\tilde{T}_{inc}(\omega, a, \theta, k_{zm}) + \tilde{T}_{ref}(\omega, a, \theta, k_{zm}) = 0 \quad (20)$$

Substituting Eqs. (12), (13) and (14) into the above condition gives the following,

$$A_n = \frac{\frac{i}{4k_1} (-1)^n \varepsilon_n H_n(k_{\alpha_1} r_0) J_n(k_{\alpha_1} a)}{H_n(k_{\alpha_1} a)} \quad (21)$$

5 Applications

The analytical expressions were used to compute the heat field generated by a point heat source placed in an unbounded solid medium (concrete) where a cylindrical circular cavity or a cylindrical circular inclusion (steel) is buried. The source, at point O $(z = 0.0 \, \text{m})$, generates a spherical heat pulse at time $t = 1.46 \text{h}$. Fig. 4a gives the plot of the spherical heat pulse as it propagates away from O with a power that increases linearly from $0 \, \text{W}$ to $1000.0 \, \text{W}$. In all the analyses, the thermal conductivity ($k_1 = 1.4 \, \text{W.m}^{-1}.^o\text{C}^{-1}$), the density ($\rho_1 = 2300 \, \text{Kg.m}^{-3}$) and the specific heat ($c_1 = 880.0 \, \text{J.Kg}^{-1}.^o\text{C}^{-1}$) of the concrete host medium remain the same. The steel inclusion has the following properties: thermal conductivity (k_2) of $63.9 \, \text{W.m}^{-1}.^o\text{C}^{-1}$; density ($\rho_2$) of 7832Kg.m^{-3}, and specific heat (c_2) of $434.0 \, \text{J.Kg}^{-1}.^o\text{C}^{-1}$. The frequency range for the analyses was $(0, 128 \times 10^{-5} \, \text{Hz})$, with increments of $1 \times 10^{-5} \, \text{Hz}$, to give a time of $(T = 27.78 \, \text{h})$ for the time domain analysis, while $L = 2\sqrt{k_2/(\rho_2 \, c_2 \Delta f)} = 28 \, \text{m}$ represents the spatial period.

The first examples assumed null fluxes (Fig. 5) or null temperatures (Fig. 6) along the boundary of the circular cavity. In each case the responses are registered at
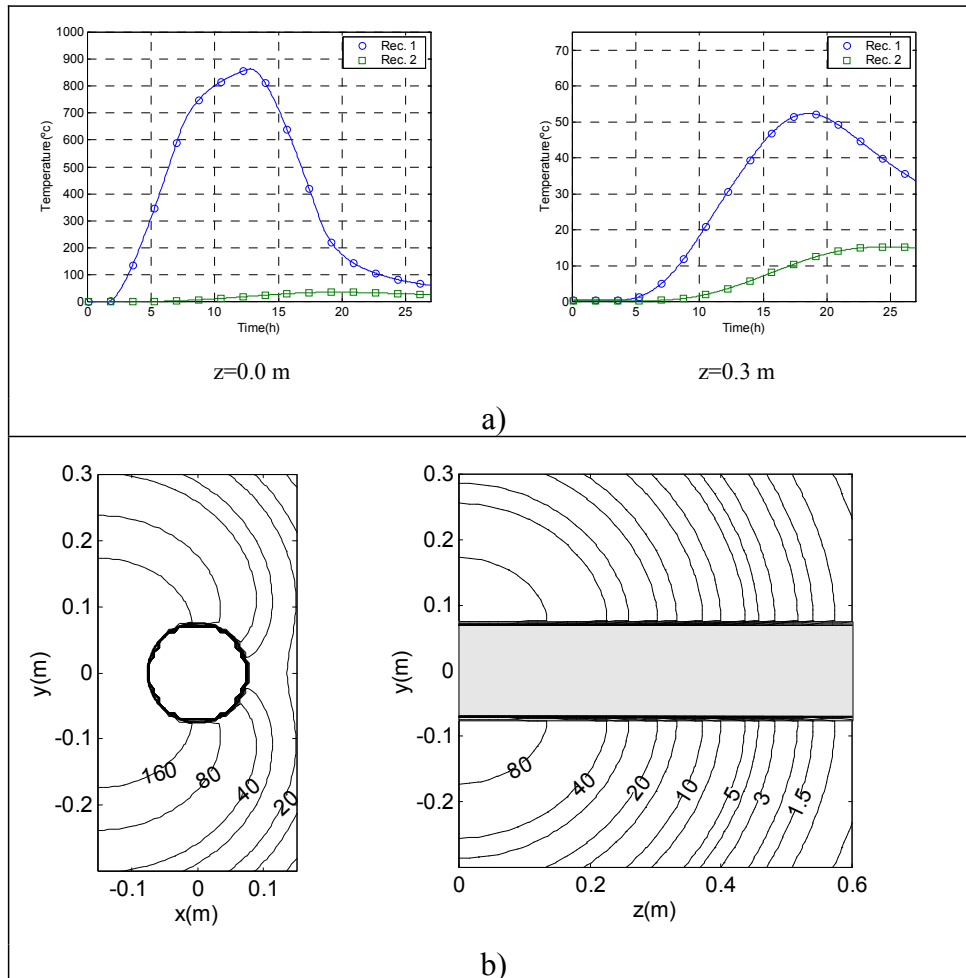
Figure 5 : Homogeneous concrete medium with a circular inclusion with null fluxes along its boundary: a) Heat curves registered at Rec. 1 and Rec. 2 for different z coordinates b) Temperature fields registered at the two grids of receivers for $t = 15$ h.

receivers Rec. 1 and Rec. 2 for different z positions ($z = 0.0$ m and $z = 0.3$ m). When $t = 15$ h snapshots displaying the temperature field along a transversal grid of receivers placed at $z = 0.0$ m and a longitudinal grid of receivers placed at $x = 0.0$ m are also presented. In all cases, the temperature is held to be null at the beginning of the time response, and once the source is activated, at ($t = 1.46$h), responses recorded by the receivers show a steady increase in temperature.

The first receivers to record a temperature change are those at $z = 0.0$ m (Fig. 5a), and Receiver 1, nearest to the heat source, is the first of these to register temperature changes. The energy emitted by the point source increases from 0 W to 1000.0 W, causing the temperature

to rise at an even rate until it reached a maximum power output of almost 700°C (at $t = 6.94$ h). When the power emitted by the source is kept at 1000.0 W, the rise in temperature continues, but more slowly, with a maximum of 880°C being attained at $t = 12.48$ h. The power is then allowed to fall until energy emission ceases altogether, and a state of equilibrium is eventually established as the energy continues to propagate from warmer to cooler regions.

Comparing the response at this receiver with that computed at receiver Rec. 2, placed in the other side of the cavity, it is clear that the latter reaches much lower temperatures, not only because it is placed further away from the source but also because of the condition of null fluxes
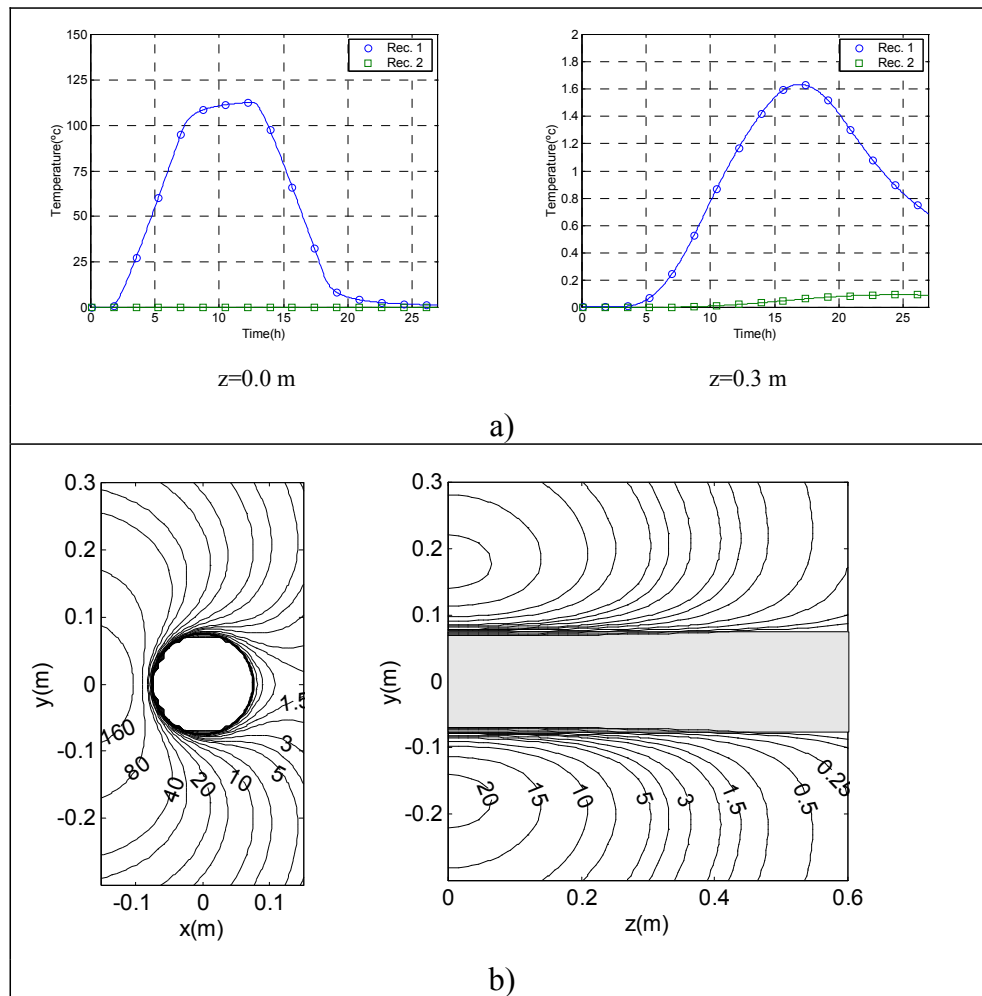
Figure 6 : Homogeneous concrete medium with a circular inclusion with null temperatures along its boundary: a) Heat curves registered at Rec. 1 and Rec. 2 for different z coordinates. b) Temperature fields registered at the two grids of receivers for $t = 15$ h.

along the boundary of the inclusion.

The null flux condition assumed for the boundary means that the cavity is now acting as a thermal insulator, and the heat energy is being concentrated between the source and the cavity, with the result that the temperature rises significantly in that region. But the cavity prevents much energy from reaching the zone behind the cavity, so scarcely any rise in temperature occurs there. These results are confirmed by those registered in the transversal grid of receivers at $t = 15$ h (see Fig. 5b).

When the receivers are placed at $z = 0.3\ m$ the temperature values registered at receivers Rec. 1 and Rec. 2 decrease in relation to the ones registered at $z = 0.0\ m$.

In addition, when $z = 0.3\ m$ the responses at the two receivers tend to aproximate. The 3D geometry of the problem means that further along z, the concentration of energy is not so high, and the solution becomes similar to that for an infinite homogeneous medium. The results registered at the longitudinal grid of receivers (see Fig. 5b) corroborate these findings. Moreover, as null fluxes are prescribed at the boundary, the isothermal lines are perpendicular to the boundary of the cavity.

When null temperature is assumed for the cavity's boundary, the results are very different (Figs. 6a and 6b). Temperature values at Rec. 1 are still higher than those at Rec. 2, but they do not reach anything like the values seen in the previous situation, because receiver
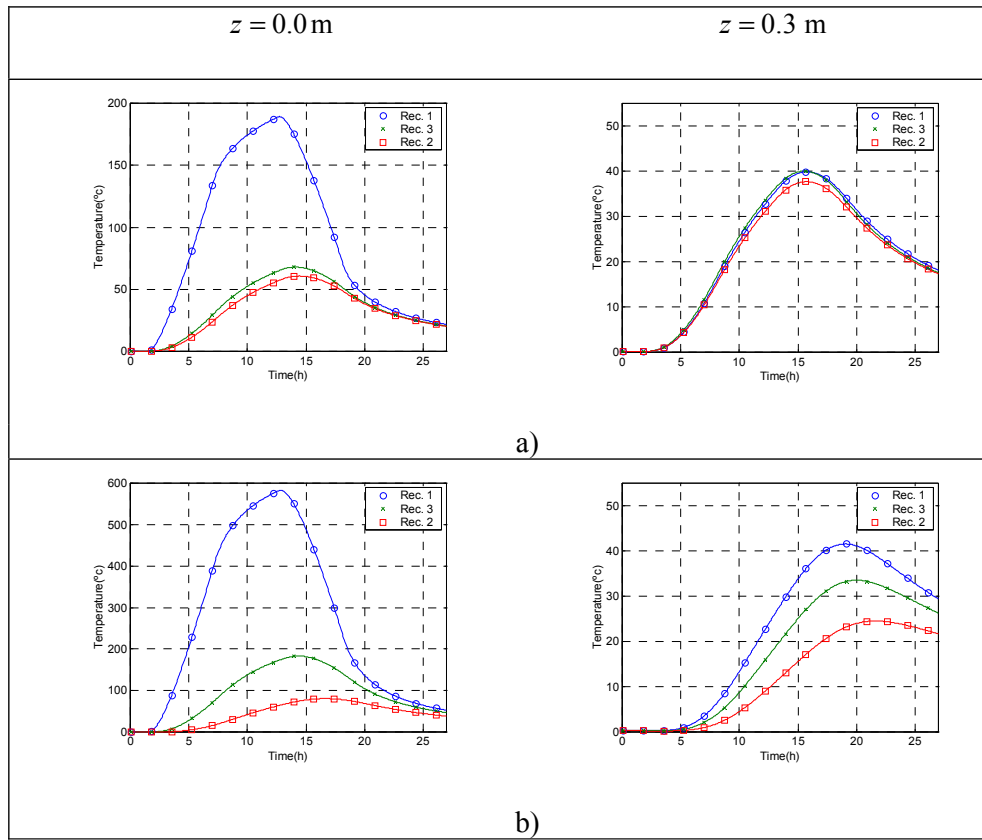
Figure 7 : Heat curves registered at Rec. 1, Rec. 2 and Rec. 3 for different z coordinates: a) homogeneous Concrete medium with a Steel circular inclusion; b) infinite homogeneous concrete medium.

Rec. 1 is now placed next to a surface with null temperature. Looking at more distant positions in *z*, the values recorded at Rec. 1 fall sharply, to a point below 1.8°, at a distance of only $z = 0.3$ m. Receiver Rec. 2, however, is both near a null temperature boundary and behind the inclusion, relative to the source, and so the temperatures recorded at this receiver are very low. The results agree with those shown in the longitudinal grid with the lowest temperatures being recorded at the receivers furthest away in *z*.

Fig. 7a illustrates the results registered at receivers Rec. 1, Rec. 2 and Rec. 3 (placed at $z = 0.0$ m and $z = 0.3$ m) when the cylindrical inclusion is made of steel. These results are compared with those computed for an infinite homogeneous medium (concrete), at the same receivers (Fig. 7b), to show the physics of the problem more clearly.

Once again the first receivers to register a temperature change are those placed at $z = 0.0$ m. As expected the

temperature curve registered at Rec. 1 exhibits a tendency similar to that registered in Fig. 5a, but with lower amplitudes since part of the energy is now transmitted to the steel inclusion. Receiver Rec. 3, which is inside the steel inclusion, records much lower temperatures than Receiver Rec. 1, for two reasons. First, Rec. 3 is further from the heat source, and second, steel has a much higher diffusivity, so that whatever energy reaches the steel disperses throughout the cylinder more quickly than it does in the host medium, with the result that the temperatures recorded are lower, but more even. Receiver Rec. 2 shows temperature increases that are similar to those recorded within the steel inclusion, indicating the influence of the steel cylinder.

Comparison with the responses for an infinite concrete medium corroborates the results observed. The Rec. 1 temperature curve for the infinite medium is similar to that plotted for the case of the steel inclusion, but the maximum temperature recorded is 3.0 times higher. This
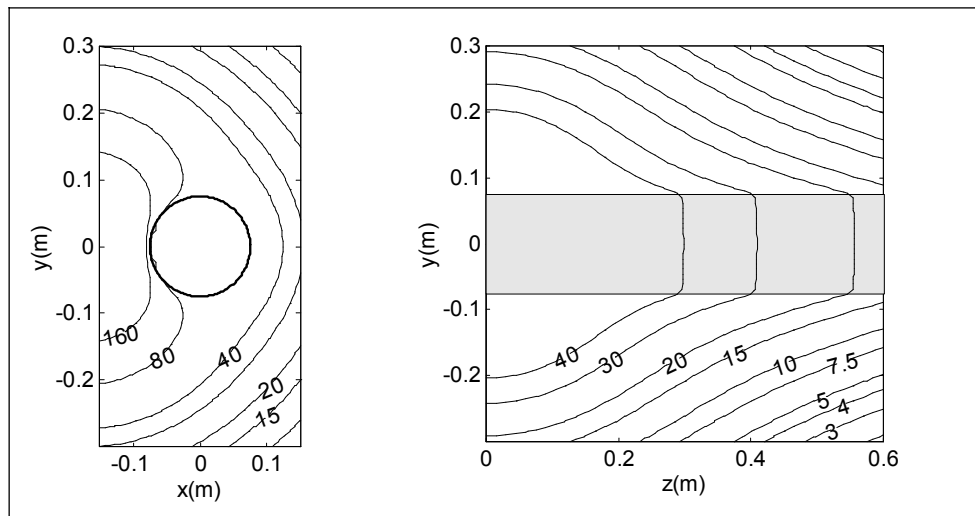
Figure 8 : Homogeneous Concrete medium with a Steel circular inclusion. Temperature fields registered at the two grids of receivers $t = 15$ h.

is because there is only one set of physical properties to consider: those of the concrete, which is the host medium. The heat thus tends to build up in the zones nearest the source since it propagates much more slowly in this medium. Receiver Rec. 3 registers the same phenomenon, with the highest temperatures recorded being 1.3 higher than those of the case that assumes the existence of the steel inclusion. The difference between the maximum temperature registered at receivers Rec. 1 and Rec. 3 is more evident in the infinite homogeneous concrete medium since the presence of the steel inclusion enables more energy to pass more quickly to the zone behind it.

In the case of a cylindrical steel inclusion, the temperature evolution for all three receivers located at $z = 3.0$ m differs only slightly, since the heat largely propagates via the most conductive material, i.e. the steel. For the case of the infinite homogeneous medium, and at the same receivers, there was a distinct temperature evolution which was strongly dependent on the distance between the source and the receiver. Since concrete has lower diffusivity than steel, it took longer for the maximum temperatures to be reached.

Fig. 8 shows the contour snapshots, at $t = 15$ h of the temperature values registered by a transversal grid of receivers along $z = 0.0$ m and a longitudinal grid of receivers located at $x = 0.0$ m.

The energy propagating from the source disperses through the medium. It travels less quickly outside the steel cylinder than it does longitudinally, and so the zones separated from the source by the inclusion record higher temperatures at the transverse line of receivers than other zones, even though they are the same distance from the source. At $t = 15$ h, the power of the source is declining. In the plane of the source ($z = 0.0$ m) the receivers placed near it show a fall in temperature, whereas receivers further from the source register temperatures that are increasing or reaching a maximum. The steel cylinder has permitted a considerable amount of energy to reach receivers that are quite a long way from the emitting source, even ones placed at $z = 0.6$ m as can be seen from the values registered by the longitudinal grid. When the source ceases to emit energy (0 W), the energy within the media continues to propagate, and the receivers placed further from the source record a rise in temperature, while those nearer to it register a decline (not illustrated).

6   Conclusions

The work described here concerns the use of a discrete integration over wavenumbers and frequencies to compute the 3D heat field originated when heat point sources are placed in the vicinity of a cylindrical circular inclusion in an unbounded solid medium. The dis-

cretization of the wavenumber-frequency integral transform presented is the mathematical equivalent of a periodic sequence of sources, parallel to the axis of the cylinder, that are also periodic in time.

Complex frequencies were used to counteract the effects of the periodicities.

This method was then applied to the problem of heat conduction within unbounded solid media, in the presence of a cylindrical circular cavity or a cylindrical circular solid inclusion. The results indicate that the method could usefully be adopted to analyse 3D thermal propagation where the geometry is 2D. Considerable differences in behaviour were found for the cases of a solid inclusion, a cavity with the imposition of null surface temperature, and a cavity assumed to have null normal surface fluxes. The imposition of boundary conditions showed that the temperature field was strongly influenced by such conditions.

References

Bouchon, M.; Aki, K. (1977): Discrete wavenumber representation of seismic-source wave field, *Bulletin of the Seismological Society of America* 67 259-277.

Carslaw, H. S.; Jaeger, J. C. (1959): Conduction of Heat in Solids, second edition, Oxford University Press.

Godinho, L.; António, J.; Tadeu, A. (2001): 3D sound scattering by rigid barriers in the vicinity of tall buildings, *Journal of Applied Acoustics* 62(11) 1229-1248.

Phinney, R. A. (1965): Theoretical calculation of the spectrum of first arrivals in layered elastic medium, *J. Geophys. Res.* 70 5107-5123.

Tadeu, A.; Antonio, J.; Simoes, N. (2004): 2.5D Green's functions in the frequency domain for heat conduction problems in unbounded, half-space, slab and layered media, *CMES: Computer Modeling in Engineering & Sciences*, vol. 6, no. 1, 43-58.

Tadeu, A.; Godinho, L.; Santos, P. (2002): Wave motion between two fluid filled boreholes in an elastic medium, *Engineering Analysis with Boundary Elements - EABE* 26(2) 101-117.

Tadeu, A.; Kausel, E. (2000): Green's functions for two-and-a-half dimensional elastodynamic problems, *Journal of Engineering Mechanics* – ASCE 126(10) 1093-1097.

Watson, G. N. (1980): A Treatise on the Theory of Bessel Functions, second edition, Cambridge University Press.